Strong Terahertz Radiation via Rapid Polarization Reduction in Photoinduced Ionic-To-Neutral Transition in Tetrathiafulvalene-*p*-Chloranil

Yuto Kinoshita,[1] Noriaki Kida,[1] Yusuke Magasaki,[1] Takeshi Morimoto,[1] Tsubasa Terashige,[2] Tatsuya Miyamoto,[1] and Hiroshi Okamoto[1,2]

[1]*Department of Advanced Materials Science, The University of Tokyo, 5-1-5 Kashiwa-no-ha, Chiba 277-8561, Japan*

[2]*AIST-UTokyo Advanced Operando-Measurement Technology Open Innovation Laboratory, National Institute of Advanced Industrial Science and Technology, Chiba 277-8568, Japan*

(Received 7 October 2018; revised manuscript received 6 May 2019; accepted 8 January 2020; published 6 February 2020)

Terahertz lights are usually generated through the optical rectification process within a femtosecond laser pulse in noncentrosymmetric materials. Here, we report a new generation mechanism of terahertz lights based upon a photoinduced phase transition, in which an electronic structure is rapidly changed by a photoirradiation. When a ferroelectric organic molecular compound, tetrathiafulvalene-*p*-chloranil, is excited by a femtosecond laser pulse, the ionic-to-neutral transition is driven and simultaneously a strong terahertz radiation is produced. By analyzing the terahertz electric-field waveforms and their dependence on the polarization direction of the incident laser pulse, we demonstrate that the terahertz radiation originates from the ultrafast decrease of the spontaneous polarization in the photoinduced ionic-to-neutral transition. The efficiency of the observed terahertz radiation via the photoinduced phase transition mechanism is found to be much higher than that via the optical rectification in the same material and in a typical terahertz emitter, ZnTe.

DOI: 10.1103/PhysRevLett.124.057402

Recent developments in the generation and detection techniques of a terahertz electromagnetic wave or a terahertz pulse have opened a new possibility for their various applications such as imaging, sensing, and spectroscopy [1,2]. The exploration of a strong terahertz-radiation source becomes important in developing terahertz science and technology. Within the classical electromagnetism, a generation of a terahertz pulse can be understood as the electric-dipole radiation, which is given by

$$\boldsymbol{E}_{\mathrm{THz}} \propto \frac{\partial^2}{\partial t^2}\boldsymbol{P}. \tag{1}$$

Here, $\boldsymbol{E}_{\mathrm{THz}}$ is the electric field of the generated terahertz pulse and $\boldsymbol{P}$ is the time-dependent polarization. In this framework, a most popular generation mechanism is an optical rectification (OR) [3] or, equivalently, a difference frequency generation (DFG) within a femtosecond laser pulse via the second-order optical nonlinearity [4]. The induced nonlinear polarization is expressed by $P_i^{(2)} = \epsilon_0 \chi_{ijk}^{(2)} E_j^{\omega} E_k^{\omega *}$, in which $\chi_{ijk}^{(2)}$ is the second-order nonlinear susceptibility, ϵ_0 is the vacuum permittivity, and E^{ω} is the light electric field [4]. As a femtosecond laser source, an output of a titanium-sapphire (TS) laser (a wavelength of 800 nm and a photon energy of 1.55 eV) with a temporal width of 100 fs, is frequently used. That pulse has a finite spectral width of ~5 THz, and the DFG can occur within the pulse from the nonlinear polarization $P^{(2)}$. This results in the generation of a broadband terahertz pulse with the central frequency of ~1 THz, the electric-field waveform of which is almost proportional to the second time derivative of the envelope of the incident femtosecond laser pulse [1,5,6]. Using this process in a transparent media with no space inversion symmetry, e.g., inorganic crystals [1,7,8] such as ZnTe and organic crystals [9,10] such as 4-*N*,*N*-dimethylamino-4′-*N*′-methyl stilbazolium tosylate (DAST), a stable terahertz pulse can be obtained. In the OR process, however, it is difficult to enhance the electric-field amplitude of a generated terahertz pulse, since two-photon absorption of an incident femtosecond laser pulse necessarily occurs, which limits the pulse fluence introduced to the nonlinear optical crystal. To overcome this difficulty, the pulse-front-tilting method using a TS regenerative amplifier (TSRA) and a wide-gap nonlinear optical crystal $LiNbO_3$ [2], and another DFG method [11,12] combining an organic nonlinear optical crystal, 4-*N*, *N*-dimethylamino-4′-*N*′-methyl-stilbazolium 2,4,6-trimethylbenzenesulfonate (DSTMS) and a near-IR femtosecond laser pulse have been proposed, although they require a special optical setup and a strong near-IR laser source different from TSRA, respectively.

In this Letter, we report a new generation mechanism of a strong terahertz pulse using a photoinduced phase transition (PIPT), in which a ferroelectric phase is melted by the irradiation with a femtosecond laser pulse. In the PIPT, a macroscopic polarization is rapidly decreased, which can

induce a strong terahertz radiation via Eq. (1). The studied material is a mixed-stacked organic molecular compound, tetrathiafulvalene-*p*-chloranil (TTF-CA), which is one of the most famous compounds showing PIPTs [13–17]. We demonstrate that the efficiency of the terahertz radiation via the PIPT in TTF-CA is much higher than that via the OR in a typical terahertz emitter, ZnTe.

Figure 1(a) shows the crystal structure of TTF-CA. Donor (D) TTF and accepter (A) CA molecules stack alternately along the a axis, resulting in the formation of the quasi-one-dimensional electronic structure. The electronic state is characterized by the degree of charge transfer (CT), ρ, from the A to D molecules [18]. At room temperature, TTF-CA is a van der Waals neutral crystal [Fig. 1(b)] with $\rho_N \sim 0.3$. With decreasing temperature, it undergoes the neutral (N) -to-ionic (I) phase transition at $T_c = 81$ K and ρ increases ($\rho_I \sim 0.6$) [19–21]. The I phase is stabilized by the energy gain because of the long-range Coulomb attractive interaction or the Madelung potential. The lattice contraction caused by the decrease of temperature enhances the Madelung potential, which drives the NI transition [19,20,22]. In the I phase, each molecule has a spin $1/2$, so that DA molecules are dimerized as shown by the ellipses in Fig. 1(c) because of the spin-Peierls-like instability. The dimeric molecular displacements are three-dimensionally ordered, breaking the space inversion symmetry along the a axis [20,22]. The recent measurement of the polarization–electric-field characteristic demonstrates that TTF-CA

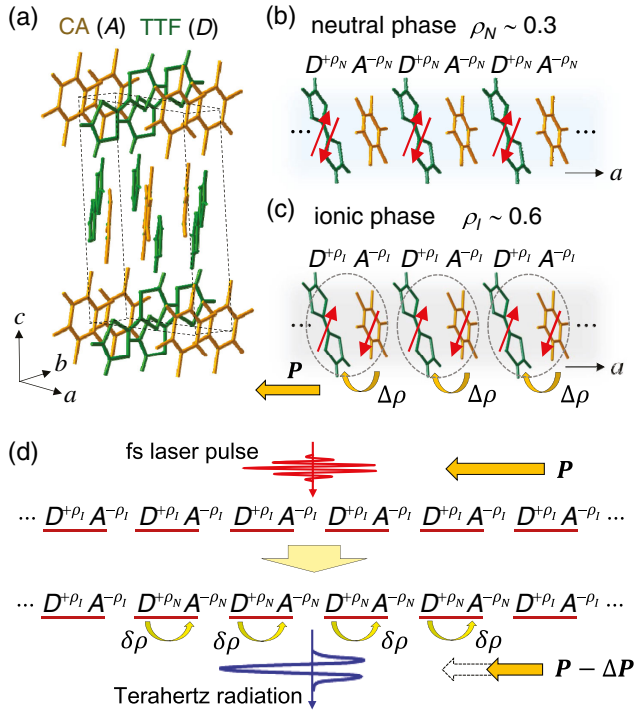

FIG. 1. (a) Crystal structure of TTF-CA. (b),(c) Molecular stacks in (b) neutral and (c) ionic phases. (d) Schematic of the ionic-to-neutral transition induced by a femtosecond laser pulse and terahertz radiation via the polarization reduction.

shows a spontaneous polarization P_S along the a axis in the I phase [23]. It is also revealed that the direction of P_S is antiparallel (parallel) to the displacement direction of $D^{+\rho}$ ($A^{-\rho}$) molecules as shown by the yellow arrow in Fig 1(c). These results indicate that P_S is not caused by the displacement of the ionic molecules [23] but originates from the collective intradimer electron transfers. In fact, the magnitude of P_S is 6.3 μC/cm^2, which is about 20 times larger than that estimated from the point-charge model [23–25]. This type of ferroelectricity is called electronic ferroelectricity.

This NI transition can also be induced by a photoirradiation. When TTF-CA is irradiated with a femtosecond laser pulse below T_c, the I state is converted to the N state [14,16,26], which is called a photoinduced I-to-N transition. The formation process of the N state has been investigated by both theoretical [27,28] and experimental studies [14,16,26,29]. The pump-probe reflection spectroscopy suggested that by exciting TTF-CA in the I phase with the resonance to the lowest CT transition at 0.65 eV, the $D^{\rho_N} A^{\rho_N}$ pair is initially generated. It makes the surrounding I states within the DA stack unstable and converts them to the N states as schematically shown in Fig. 1(d) [16]. The size of the N domain thus produced was estimated to be $\sim 8 D^{\rho_N} A^{\rho_N}$ pairs per photon at low temperatures, far below T_c. The initial I-to-N conversion processes occur within 20 fs and are considered to be purely electronic in nature [26]. Such an I-to-N conversion decreases the ferroelectric polarization as ascertained by the optical-pump second-harmonic-generation-probe measurements [29]. This makes us expect the strong terahertz radiation during the photoinduced I-to-N transition.

(001)-oriented single crystals were grown by the co-sublimation method [16]. The cleaved (001)-surface with the thickness of ~250 μm was obtained and was cooled with a rate of 0.33 K/ min to avoid a clacking of the crystal.

For terahertz-radiation experiments, an optical parametric amplifier excited by an output of a TSRA (central wavelength of 800 nm, repetition rate of 1 kHz, temporal width of 100 fs) was used. The excitation pulse is set at 0.65 eV corresponding to the CT transition, and focused on the sample in the normal incidence. The penetration depth of the 0.65-eV light is ~40 nm at 15 K [16], which is much shorter than the typical thickness of samples (~150–300 μm), and only the surface region is photoexcited. To avoid absorptions of the terahertz radiation by infrared-active phonons [30–33], we use the reflection configuration [Fig. 2(a)] [34]. Electric-filed waveforms of generated terahertz pulses along the a axis are measured by a standard electro-optic (EO) sampling with a 1-mm-thick (110) ZnTe crystal. We confirmed that emitted terahertz pulses are polarized along the a axis. By using terahertz-radiation imaging [35,36], we confirmed that the TTF-CA crystal consists of a single ferroelectric domain (Supplemental Material, S1 [37]).

A typical electric-field waveform of a terahertz pulse generated by the 0.65-eV excitation at 15 K is shown in

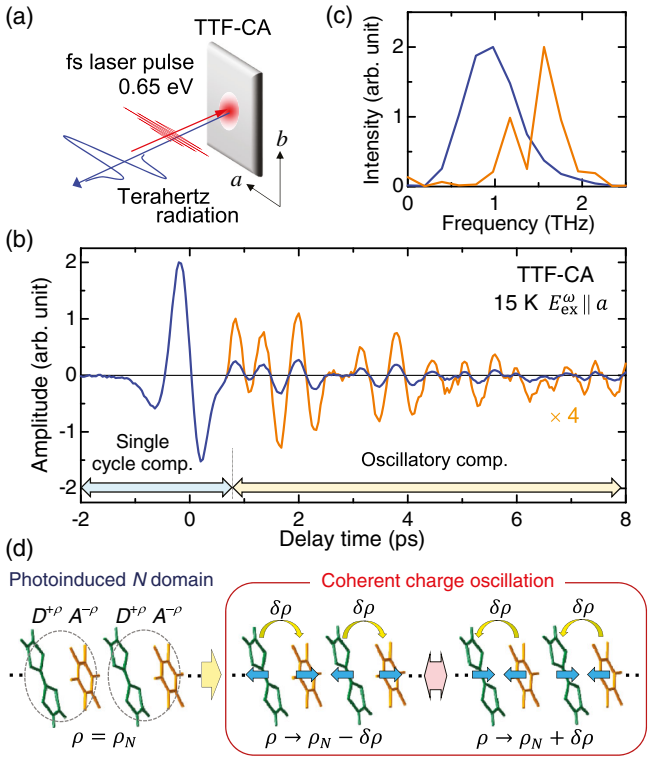

FIG. 2. (a) Schematic of terahertz-radiation measurement. (b) Terahertz electric-field waveform for $E^{\omega}_{ex} \| a$, measured at 15 K. (c) Normalized Fourier power spectra of the data shown in (b); the blue (orange) line shows the single-cycle component at −2 to 0.8 ps (the oscillatory component at 0.8 to 8 ps). (d) Schematic of a coherent charge oscillation in a photoinduced N domain originating from the release of the dimerization.

Fig. 2(b) (the blue line). The excitation photon density per unit area was 1.6×10^{15} photon/cm^2. Within the penetration depth, the excitation density is estimated to be 0.11 photon/DA pair. The incident electric field of a femtosecond laser pulse is set parallel to the a axis ($E^{\omega}_{ex} \| a$). In our experiments, we cannot determine the time origin (0 ps), which should be defined as the time when the incident laser pulse reaches the sample. Instead, we set the time origin at the time when the absolute value of the terahertz electric field $|E_{THz}(t)|$ for $E^{\omega}_{ex} \| b$ ($E^{\omega}_{ex} \perp a$) is the maximum, as discussed later. The generated terahertz pulse consists of a single-cycle component around 0 ps and the subsequent oscillatory component.

The blue line in Fig. 2(c) displays the Fourier power spectrum of the single-cycle component in the range of −2.0–0.8 ps indicated by an arrow in Fig. 2(b). It shows the peak structure at ∼0.98 THz and expands to ∼2.20 THz. The orange line shows the Fourier power spectrum of the oscillatory component in the range of 0.8–8 ps, which exhibits a peak structure at 1.60 THz (∼53 cm^{-1}). The tiny dip at ∼1.37 THz is due to the absorption of quartz used for a cryostat window, which is detailed in the Supplemental Material S2 [37]. In order to characterize the magnitude of the terahertz electric field in TTF-CA, we measured the terahertz electric-field waveform in a (110)-oriented ZnTe crystal in the same experimental setup. ZnTe is known to show a strong terahertz radiation via the optical rectification (OR) mechanism. The results reveal that the maximum amplitude (intensity) of the terahertz electric field in TTF-CA is at least 25 (600) times as large as that in ZnTe (Supplemental Material S3 [37]).

To reveal the terahertz-radiation mechanism in TTF-CA, we measured how the terahertz electric-field waveform depends on the direction of the light electric field E^{ω}_{ex} of the incident femtosecond pulse. Figures 3(a) and 3(b) show the terahertz electric-field waveforms with $E_{THz}(t) \| a$ at 15 K for $E^{\omega}_{ex} \| a$ and $E^{\omega}_{ex} \| b$ ($E^{\omega}_{ex} \perp a$), respectively. The excitation photon density was 1.6×10^{15} photon/cm^2 in common. The time origin is set at the time when $|E_{THz}(t)|$ for $E^{\omega}_{ex} \| b$ is the maximum. The maximum value of $|E_{THz}(t)|$ for $E^{\omega}_{ex} \| b$ is about 1/2.5 of that for $E^{\omega}_{ex} \| a$. Noticeably, the observed waveform for $E^{\omega}_{ex} \| b$ [Fig. 3(b)] is considerably different from that for $E^{\omega}_{ex} \| a$ [Fig. 3(a)]. As guided by dotted vertical lines at 0 ps, $|E_{THz}(0)|$ is nearly equal to zero for $E^{\omega}_{ex} \| a$, when $|E_{THz}(0)|$ is the maximum for $E^{\omega}_{ex} \| b$. The Fourier power spectrum obtained using the waveform from −2.0 to 0.8 ps for $E^{\omega}_{ex} \| b$ shows the peak at ∼0.60 THz [as shown later in Fig. 4(b)], which is slightly lower than the peak (0.98 THz) for $E^{\omega}_{ex} \| a$ [Fig. 2(c)].

The observed polarization dependence of the electric-field waveforms suggests that two different mechanisms of terahertz radiations exist in TTF-CA. Since the sample is transparent for the 0.65-eV light with $E^{\omega}_{ex} \| b$, the terahertz radiation for $E^{\omega}_{ex} \| b$ can be ascribed to the OR mechanism. For 0.65-eV light with $E^{\omega}_{ex} \| a$, the PIPT occurs. Therefore, it

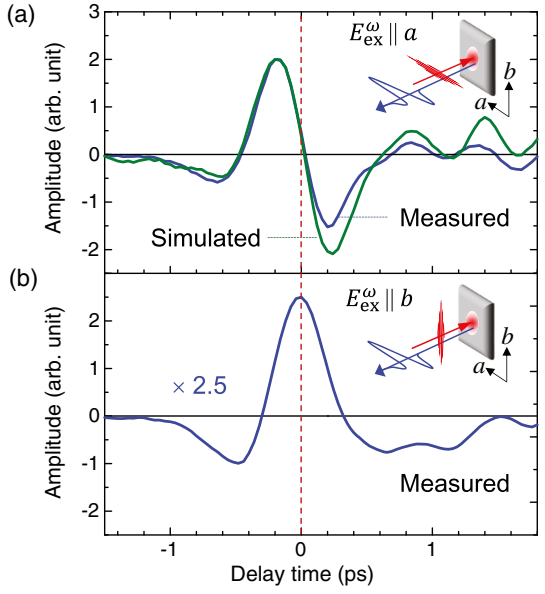

FIG. 3. Measured terahertz electric-field waveforms for (a) $E^{\omega}_{ex} \| a$ and (b) $E^{\omega}_{ex} \| b$, respectively. Simulated waveform is shown by the green line.

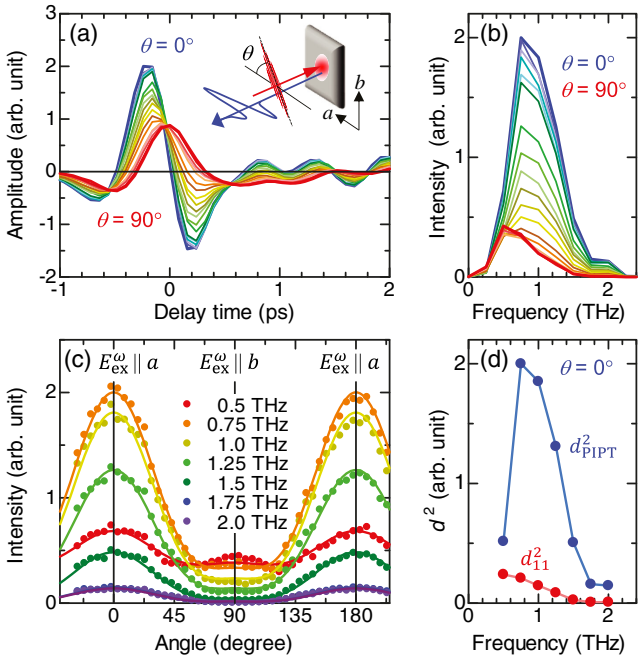

FIG. 4. Light-polarization angle θ dependence of (a) terahertz electric-field waveforms and (b) their Fourier power spectra. (c) Intensities at various frequencies as a function of θ. (d) Frequency dependence of the square of the d tensor originating from optical rectification (d_{11}^2) and photoinduced phase transition ($d_{\mathrm{PIPT}}{}^2$).

is natural to consider that the terahertz radiation for $E_{\mathrm{ex}}^{\omega} \| a$ is attributed to the decrease of the ferroelectric polarization in the photoinduced I-to-N transition (the PIPT mechanism).

To ascertain this interpretation, we next simulated the terahertz electric-field waveform via the PIPT mechanism. Here, it should be considered that an electric-field waveform experimentally obtained is affected by the frequency dependence of the detection sensitivity in the EO sampling. In our study, we correct it by considering the electric-field waveform for $E_{\mathrm{ex}}^{\omega} \| b$, the generation mechanism of which is OR. By comparing the experimental electric-field waveform with the theoretical one, we can determine a response function $\beta(\omega)$ of our measurement system. The derivation of $\beta(\omega)$ and the simulation of the terahertz radiation are detailed in the Supplemental Material S4 [37]. If the OR mechanism is dominant, the ideal amplitude spectrum of the terahertz electric field is proportional to the Fourier power spectrum of the second time-derivative of $P^{(2)}$, which is given by $E_{\mathrm{THz}}^{\mathrm{OR}}(\omega) \propto (i\omega)^2 I(\omega)$, where $I(\omega)$ is a Fourier power spectrum of an envelope function of the incident laser pulse [5,6]. On the other hand, if the PIPT is dominant, the ideal amplitude spectrum of the electric field is given by $E_{\mathrm{THz}}^{\mathrm{PIPT}}(\omega) \propto (i\omega)^2 I(\omega)[1/(i\omega + a)]$, which includes a relaxation function with a time constant $1/a$. By using $\beta(\omega)$, we simulate the terahertz electric-field waveform originating from the PIPT, which is shown by the green line in Fig. 3(a). The simulated waveform successfully reproduces the characteristic feature that $|E_{\mathrm{THz}}(0)|$ is zero for $E_{\mathrm{ex}}^{\omega} \| a$ [Fig. 3(a)] when $|E_{\mathrm{THz}}(0)|$ is maxima for $E_{\mathrm{ex}}^{\omega} \| b$ [Fig. 3(b)].

The coherent oscillation [orange line in Fig. 2(a)] is observed only for $E_{\mathrm{ex}}^{\omega} \| a$, which is detailed in the Supplemental Material S5 [37], and can also be related to the PIPT. A similar oscillation was observed in the reflectivity change at the intramolecular transition band of TTF in the visible region during the photoinduced I-to-N transition [16,26,45] and assigned to the coherent oscillation corresponding to the release of the dimerization in the photogenerated N domains. This coherent oscillation of the dimeric mode slightly modulates the degree of CT ρ_N in the photogenerated N states as $\rho_N \pm \delta\rho$, which is schematically shown in Fig. 2(d). Such a charge modulation gives rise to the terahertz radiation with the same frequency.

In order to further discuss the terahertz-radiation mechanism in TTF-CA, we measured the electric-field waveforms of the terahertz radiations by changing the polarization angle θ of the incident pulse with a step of 5°. The results and their Fourier power spectra are shown in Figs. 4(a) and 4(b), respectively. By changing θ from 0° to 90°, the central frequency of the spectrum is shifted to the lower frequency, while the peak intensity decreases. In order to see this tendency, we plotted the magnitudes of the terahertz-radiation intensities at selected frequencies as a function of θ (0° to 180°) in Fig. 4(c). The intensity reaches the maxima at $\theta = 0°$ and $\theta = 180°$ ($E_{\mathrm{ex}}^{\omega} \| a$) and the intensity below 1.5 THz is finite at $\theta = 90°$ ($E_{\mathrm{ex}}^{\omega} \| b$).

We can also simulate the observed θ dependence of the terahertz-radiation intensity. As mentioned above, the PIPT occurs only for $E_{\mathrm{ex}}^{\omega} \| a$ in TTF-CA [16]. In this case, the terahertz-radiation intensity along the a axis, I_a^{PIPT}, is expressed as

$$I_a^{\mathrm{PIPT}} = |E_a^{\mathrm{PIPT}}|^2 \propto d_{\mathrm{PIPT}}^2 \cos^4\theta E_0^4. \tag{2}$$

Here, d_{PIPT} is the coefficient characterizing the terahertz-radiation efficiency and E_0 is the electric field of the incident light. The fitting curves based on Eq. (2) cannot reproduce the finite intensity at $\theta = 90°$ ($E_{\mathrm{ex}}^{\omega} \| b$) (Fig. S9 in the Supplemental Material S6 [37]). To discuss the θ dependence of the terahertz radiation via the OR mechanism, the symmetry analysis is necessary. TTF-CA in the I phase has the point group m and the d tensor can have finite values of d_{11}, d_{12}, d_{13}, and d_{16} in our experimental configuration [inset of Fig. 4(a)] [4]. The terahertz-radiation intensity polarized along the a axis due to OR, I_a^{OR}, is expressed as

$$I_a^{\mathrm{OR}} = |E_a^{\mathrm{OR}}|^2 \propto |(d_{11}\cos^2\theta + d_{12}\sin^2\theta)|^2 E_0^4. \tag{3}$$

Using the fitting curves based on Eq. (3) or the combination of Eqs. (2) and (3), however, we could not completely reproduce the experimental data (see Fig. S9).

We next introduced the phase difference ϕ between Eqs. (2) and (3), which gives the expression as

$$I_a = |E_a^{\mathrm{OR}} + E_a^{\mathrm{PIPT}} \exp(i\phi)|^2. \quad (4)$$

Using this formula with $\phi = 90°$ and $d_{11}/d_{12} = 3.05$, the observed θ dependence of the radiation intensity can be well reproduced as shown by thin solid lines in Fig. 4(c). Thus, we conclude that the terahertz radiation in TTF-CA can be explained by the combination of OR and PIPT mechanisms. This conclusion is also supported by the incident laser-power dependence of the terahertz-radiation intensity (Supplemental Material S7 [37]). In Fig. 4(d), we show the spectrum of the square of the d_{PIPT} (d_{11}) value characterizing the terahertz-radiation efficiency by the PIPT (OR) mechanism by blue (red) circles. The magnitude of d_{PIPT}^2 is approximately 1 order larger than that of d_{11}^2 dominating the OR. This indicates that the polarization reduction via the photoinduced I-to-N transition in TTF-CA is a very efficient mechanism as a light-induced terahertz radiation.

Finally, we mention the usefulness of the terahertz-radiation experiments to study the PIPT phenomena (see the Supplemental Material S8). Just after the photoexcitation, an N domain consisting of a number of $D^{\rho_N}A^{\rho_N}$ pairs is formed in the timescale of the transfer energy ~20 fs [16,26]. Such an initial PIPT process induces the polarization reduction, which is reflected by the shape of the terahertz electric-field waveform (Supplemental Material S4 [37]). Since we used a 100 fs laser pulse for both the photoexcitation of the system and the detection of the terahertz radiation, it was difficult to derive the information about the initial PIPT process from the terahertz electric-field waveforms. The terahertz-radiation experiments using a shorter laser pulse, e.g., with the temporal width of 20 fs, would provide valuable information about the initial PIPT process, which is a future study subject.

In summary, we observed the strong terahertz radiation via the ferroelectric polarization reduction in the photoinduced ionic-to-neutral transition of TTF-CA. The intensity of the terahertz electric field is approximately 10 times as large as that caused by optical rectification in the same sample and approximately 600 times as large as that in ZnTe. Thus, our result provides a new way for obtaining the strong terahertz radiation by the photoinduced-phase-transition mechanism, which will be able to be used for various terahertz applications.

This work was partly supported by a Grant-in-Aid by MEXT (No. JP25247058, No. JP25600072, No. JP15K13330, No. JP18H01166, and No. JP18H01858) and CREST (No. JPMJCR1661), Japan Science and Technology Agency. Y. K. and T. Morimoto were supported by Japan Society for the Promotion of Science (JSPS) through Program for Leading Graduate Schools (MERIT) and JSPS Research Fellowships for Young Scientists.

[1] M. Tonouchi, Cutting-edge terahertz technology, Nat. Photonics **1**, 97 (2007).
[2] T. Kampfrath, K. Tanaka, and K. A. Nelson, Resonant and nonresonant control over matter and light by intense terahertz transients, Nat. Photonics **7**, 680 (2013).
[3] M. Bass, P. A. Franken, J. F. Ward, and G. Weinreich, Optical Rectification, Phys. Rev. Lett. **9**, 446 (1962).
[4] Y. R. Shen, *The Principles of Nonlinear Optics* (Wiley, New York, 1984).
[5] D. H. Auston and M. C. Nuss, Electrooptic generation and detection of femtosecond electrical transients, IEEE J. Quantum Electron. **24**, 184 (1988).
[6] J. Ahn, A. V. Efimov, R. D. Averitt, and A. J. Taylor, Terahertz waveform synthesis via optical rectification of shaped ultrafast laser pulses, Opt. Express **11**, 2486 (2003).
[7] B. B. Hu, X.-C. Zhang, D. H. Auston, and P. R. Smith, Free-space radiation from electro-optic crystals, Appl. Phys. Lett. **56**, 506 (1990).
[8] A. Nahata, A. S. Weling, and T. F. Heinz, A wideband coherent terahertz spectroscopy system using optical rectification and electro-optic sampling, Appl. Phys. Lett. **69**, 2321 (1996).
[9] X.-C. Zhang, X. F. Ma, Y. Jin, T.-M. Lu, E. P. Boden, P. D. Phelps, K. R. Stewart, and C. P. Yakymyshyn, Terahertz optical rectification from a nonlinear organic crystal, Appl. Phys. Lett. **61**, 3080 (1992).
[10] J. J. Carey, R. T. Bailey, D. Pugh, J. N. Sherwood, F. R. Cruickshank, and K. Wynne, Terahertz pulse generation in an organic crystal by optical rectification and resonant excitation of molecular charge transfer, Appl. Phys. Lett. **81**, 4335 (2002).
[11] B. Monoszlai, C. Vicario, M. Jazbinsek, and C. P. Hauri, High-energy terahertz pulses from organic crystals: DAST and DSTMS pumped at Ti:sapphire wavelength, Opt. Lett. **38**, 5106 (2013).
[12] C. Vicario, M. Jazbinsek, A. V. Ovchinnikov, O. V. Chefonov, S. I. Ashitkov, M. B. Agranat, and C. P. Hauri, High efficiency THz generation in DSTMS, DAST and OH1 pumped by Cr:forsterite laser, Opt. Express **23**, 4573 (2015).
[13] S. Koshihara, Y. Tokura, T. Mitani, G. Saito, and T. Koda, Photoinduced valence instability in the organic molecular compound tetrathiafulvalene-*p*-chloranil (TTF-CA), Phys. Rev. B **42**, 6853 (1990).
[14] S. Iwai, S. Tanaka, K. Fujinuma, H. Kishida, H. Okamoto, and Y. Tokura, Ultrafast Optical Switching from an Ionic to a Neutral State in Tetrathiafulvalene-p-chloranil (TTF-CA) Observed in Femtosecond Reflection Spectroscopy, Phys. Rev. Lett. **88**, 057402 (2002).
[15] E. Collet, M. H. Cailleau, M. B. Cointe, H. Cailleau, M. Wulff, T. Luty, S. Koshihara, M. Meyer, L. Toupet, P. Rabiller, and S. Techert, Laser-induced ferroelectric structural order in an organic charge-transfer crystal, Science **300**, 612 (2003).
[16] H. Okamoto, Y. Ishige, S. Tanaka, H. Kishida, S. Iwai, and Y. Tokura, Photoinduced phase transition in tetrathiafulvalene-*p*-chloranil observed in femtosecond reflection spectroscopy, Phys. Rev. B **70**, 165202 (2004).
[17] H. Uemura and H. Okamoto, Direct Detection of the Ultrafast Response of Charges and Molecules in the

Photoinduced Neutral-to-Ionic Transition of the Organic Tetrathiafulvalene-*p*-chloranil Solid, Phys. Rev. Lett. **105**, 258302 (2010).

[18] H. M. McConnell, B. M. Hoffman, and R. M. Metzger, Charge transfer in molecular crystals, Proc. Natl. Acad. Sci. U.S.A. **53**, 46 (1965).

[19] J. B. Torrance, A. Girlando, J. J. Mayerle, J. I. Crowley, V. Y. Lee, P. Batail, and S. J. LaPlaca, Anomalous Nature of Ionic-to-Neutral Phase Transition in Tetrathiafulvalene-Chloranil, Phys. Rev. Lett. **47**, 1747 (1981).

[20] M. Le Cointe, M. H. Lemée-Cailleau, H. Cailleau, B. Toudic, L. Toupet, G. Heger, F. Moussa, P. Schweiss, K. H. Kraft, and N. Karl, Symmetry breaking and structural changes at the ionic-to-neutral transition in tetrathiafulvalene-*p*-chloranil, Phys. Rev. B **51**, 3374 (1995).

[21] S. Horiuchi, Y. Okimoto, R. Kumai, and Y. Tokura, Anomalous valence fluctuation near a ferroelectric transition in an organic charge-transfer complex, J. Phys. Soc. Jpn. **69**, 1302 (2000).

[22] M. Buron-Le Cointe, E. Collet, B. Toudic, P. Czarnecki, and H. Cailleau, Back to the structural and dynamical properties of neutral-ionic phase transitions, Crystals **7**, 285 (2017).

[23] K. Kobayashi, S. Horiuchi, R. Kumai, F. Kagawa, Y. Murakami, and Y. Tokura, Electronic Ferroelectricity in a Molecular Crystal with Large Polarization Directing Antiparallel to Ionic Displacement, Phys. Rev. Lett. **108**, 237601 (2012).

[24] G. Giovannetti, S. Kumar, A. Stroppa, J. van den Brink, and S. Picozzi, Multiferroicity in TTF-CA Organic Molecular Crystals Predicted through *ab initio* Calculations, Phys. Rev. Lett. **103**, 266401 (2009).

[25] S. Ishibashi and K. Terakura, First-principles study of spontaneous polarization in tetrathiafulvalene-*p*-chloranil (TTF-CA), Physica (Amsterdam) **405B**, S338 (2010).

[26] T. Morimoto, T. Miyamoto, and H. Okamoto, Ultrafast electron and molecular dynamics in photoinduced and electric-field-induced neutral-ionic transitions, Crystals **7**, 132 (2017).

[27] P. Huai, H. Zheng, and K. Nasu, Theory for photoinduced ionic-neutral structural phase transition in quasi one-dimensional organic molecular crystal TTF-CA, J. Phys. Soc. Jpn. **69**, 1788 (2000).

[28] T. Yi, N. Kirova, and S. Brazovskii, Dynamical patterns of phase transformations from self-trapping of quantum excitons, Physica (Amsterdam) **460B**, 73 (2015).

[29] T. Luty, H. Cailleau, S. Koshihara, E. Collet, M. Takesada, M. H. Lemée-Cailleau, M. Buron-Le Cointe, N. Nagaosa, Y. Tokura, and E. Zienkiewicz, Static and dynamic order of cooperative multi-electron transfer, Europhys. Lett. **59**, 619 (2002).

[30] M. Masino, A. Girlando, A. Brillante, R. G. Della Valle, E. Venuti, N. Drichko, and M. Dressel, Lattice dynamics of TTF–CA across the neutral–ionic transition, Chem. Phys. **325**, 71 (2006).

[31] A. Girlando, M. Masino, A. Painelli, N. Drichko, M. Dressel, A. Brillante, R. G. Della Valle, and E. Venuti, Direct evidence of overdamped Peierls-coupled modes in the temperature-induced phase transition in tetrathiafulvalene-chloranil, Phys. Rev. B **78**, 045103 (2008).

[32] M. Dressel and T. Peterseim, Investigations of the neutral-ionic phase transition in TTF-CA and its dynamics, Crystals **7**, 17 (2017).

[33] M. Masino, N. Castagnetti, and A. Girlando, Phenomenology of the neutral-ionic valence instability in mixed stack charge-transfer crystals, Crystals **7**, 108 (2017).

[34] Y. Kinoshita, N. Kida, T. Miyamoto, M. Kanou, T. Sasagawa, and H. Okamoto, Terahertz radiation by subpicosecond spin-polarized photocurrent originating from Dirac electrons in a Rashba-type polar semiconductor, Phys. Rev. B **97**, 161104(R) (2018).

[35] K. Takahashi, N. Kida, and M. Tonouchi, Terahertz Radiation by an Ultrafast Spontaneous Polarization Modulation of Multiferroic $BiFeO_3$ Thin Films, Phys. Rev. Lett. **96**, 117402 (2006).

[36] M. Sotome, N. Kida, S. Horiuchi, and H. Okamoto, Visualization of ferroelectric domains in a hydrogen-bonded molecular crystal using emission of terahertz radiation, Appl. Phys. Lett. **105**, 041101 (2014).

[37] See Supplemental Material at http://link.aps.org/supplemental/10.1103/PhysRevLett.124.057402 for the ferroelectric domain structures visualized by the terahertz radiation imaging, the effect of absorption of quartz used in the window of the cryostat, the comparison of terahertz radiations from TTF-CA and ZnTe, the simulation of terahertz radiations from TTF-CA and their Fourier power spectra, the calculation of light-polarization angle dependence of the terahertz radiations, the excitation photon-density dependence of terahertz radiations, and the terahertz radiation as a probe of the photoinduced I-to-N transition in TTF-CA, which includes Refs. [5,6,8,16,17,26,35, 36,38–44].

[38] H. Kishida, H. Takamatsu, K. Fujinuma, and H. Okamoto, Ferroelectric nature and real-space observations of domain motions in the organic charge-transfer compound tetrathiafulvalene-*p*-chloranil, Phys. Rev. B **80**, 205201 (2009).

[39] Y. Kinoshita, N. Kida, M. Sotome, R. Takeda, N. Abe, M. Saito, T. Arima, and H. Okamoto, Visualization of ferroelectric domains in boracite using emission of terahertz radiation, Jpn. J. Appl. Phys. **53**, 09PD08 (2014).

[40] S. Roberts and D. D. Coon, Far-infrared properties of quartz and sapphire, J. Opt. Soc. Am. **52**, 1023 (1962).

[41] D. Grischkowsky, S. Keiding, M. van Exter, and Ch. Fattinger, Far-infrared time-domain spectroscopy with terahertz beams of dielectrics and semiconductors, J. Opt. Soc. Am. B **7**, 2006 (1990).

[42] W. G. Spitzer and D. A. Kleinman, Infrared lattice bands of quartz, Phys. Rev. **121**, 1324 (1961).

[43] R. Kitamura, L. Pilon, and M. Jonasz, Optical constants of silica glass from extreme ultraviolet to far infrared at near room temperature, Appl. Opt. **46**, 8118 (2007).

[44] A. Schneider, M. Neis, M. Stillhart, B. Ruiz, R. U. A. Khan, and P. Günter, Generation of terahertz pulses through optical rectification in organic DAST crystals: theory and experiment, J. Opt. Soc. Am. B **23**, 1822 (2006).

[45] T. Miyamoto, H. Yada, H. Yamakawa, and H. Okamoto, Ultrafast modulation of polarization amplitude by terahertz fields in electronic-type organic ferroelectrics, Nat. Commun. **4**, 2586 (2013).